

PCFGaze: Physics-Consistent Feature for Appearance-based Gaze Estimation

Yiwei Bao, Feng Lu *

State Key Laboratory of VR Technology and Systems, School of CSE, Beihang University

{baoyiwei, fenglu}@buaa.edu.cn

Abstract

Although recent deep learning based gaze estimation approaches have achieved much improvement, we still know little about how gaze features are connected to the physics of gaze. In this paper, we try to answer this question by analyzing the gaze feature manifold. Our analysis revealed the insight that the geodesic distance between gaze features is consistent with the gaze differences between samples. According to this finding, we construct the Physics-Consistent Feature (PCF) in an analytical way, which connects gaze feature to the physical definition of gaze. We further propose the PCFGaze framework that directly optimizes gaze feature space by the guidance of PCF. Experimental results demonstrate that the proposed framework alleviates the overfitting problem and significantly improves cross-domain gaze estimation accuracy without extra training data. The insight of gaze feature has the potential to benefit other regression tasks with physical meanings.

1. Introduction

Eye gaze reveals where human attention lands, which has been widely applied in a variety of territories, such as VR/AR systems [3, 16, 27], medical analysis [4, 15, 14] and human-computer interaction [18, 36, 28]. Gaze estimation methods can be categorized into two types, model-based approaches and appearance-based approaches. Both approaches have its own pros and cons. Model-based approaches estimate gaze by modeling the anatomical structure of eyeball, which have achieved remarkable accuracy as they are in line with physical rules behind the gaze. Unfortunately, they usually require dedicated hardware such as infrared cameras and light sources. Appearance-based approaches use inexpensive web cameras, where they employ Convolutional Neural Networks (CNNs) to regress gaze direction from user face/eye images. Although these work achieve satisfactory performance within the same dataset, their accuracy severely degrades in cross-domain settings.

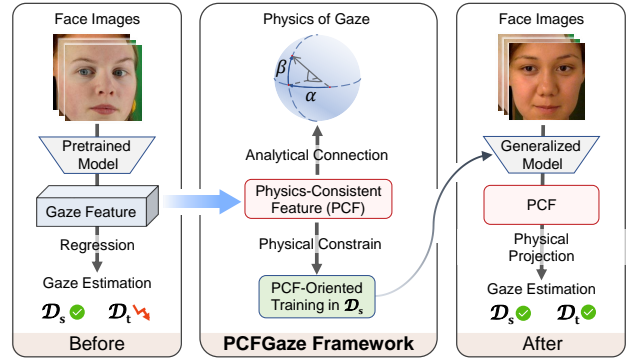


Figure 1. We propose the Physics-Consistent Feature for appearance-based gaze estimation (PCFGaze). We connect gaze feature to the physics of gaze by constructing the Physics-Consistent Feature (PCF). Then, we retrain the model in source domain by the constrain of physics provided by PCF. The generalized model estimate gaze in an analytical way and improves the generalization ability of gaze estimation models.

To improve the cross-domain performance, various domain adaptation approaches have been proposed, *i.e.*, adversarial learning [13, 34], contrastive learning [35] and collaborative learning [21]. However, these approaches require a number of target domain samples for adaptation, which is limited in real-world applications, as it is not feasible for users to collect target domain data and re-optimize the network.

On the contrary, gaze generalization approaches are user-friendly since it requires no target domain data. For example, Cheng *et al.* proposed to generalize gaze estimation model by purifying gaze feature during source domain training [6]. In fact, gaze generalization task is more challenging since the constraints from target domain is missing.

To bridge the gap between the source/target domain when the target domain data is inaccessible, we argue that the underlying principles behind the gaze in two domains should be discovered. In other words, we have to find some principles to constrain the model as an alternative of target domain data. However, such issue has been less investigated

*Corresponding Author.

in previous studies.

In this paper, we aim to address the above challenge by a simple-but-effective idea, *i.e.*, to optimize the model based on the physical rules of gaze instead of target domain data. While previous approaches are all data-driven, our idea is essentially to break the data-driven pipeline, but to introduce the physical-rule-driven approach. We believe that with the proper criteria, the extracted gaze feature is capable of revealing consistent numerical patterns of gaze. This connection helps us to constrain gaze feature by the physical rules of gaze, which alleviates the overfitting problem by reducing the dependence on ground truth data.

Following the above idea, we propose the PCFGaze framework for generalizable gaze estimation. First, we construct the Physics-Consistent Feature (PCF) based on feature obtained from pretrained model in an unsupervised manner. The proposed PCF shares the same gaze distribution pattern with the physical definitions of gaze. Second, the PCF optimizes gaze feature with source domain labels based on the physical rules of gaze to address the overfitting issue. The primary contributions of this work are as follow:

- We propose the Physics-Consistent Feature that connects gaze feature to the physical definition of gaze without label. The insight brought by PCF may also inspire other regression tasks with physical meaning.
- We propose the PCFGaze framework for generalizable gaze estimation. It estimates gaze analytically and optimizes the feature space via the physical rules of gaze.
- Experimental results illustrate that the proposed framework achieves consistent improvements in 7 different cross-dataset settings. The PCFGaze improves the generalization ability of baseline model up to 29.23% without touching target domain data.

2. Related Work

2.1. Gaze Estimation

There are two mainstream gaze estimation approaches, the model-based approach and the appearance-based approach. Model-based approaches estimate gaze by reconstructing the anatomy structure of the eyeball [12]. These methods achieve remarkable accuracy but also require personal calibration and dedicated devices such as depth sensors [29, 37], infrared cameras [30, 11] and lights [11, 20] to accurately rebuild the tiny structures like pupil and corneal.

Appearance-based approaches estimate gaze from user images captured by a single web camera. Early methods estimate gaze from eye images by traditional machine learning algorithms like manifold embedding [26] and adaptive linear regression [23]. Lu *et al.* propose to estimate eye

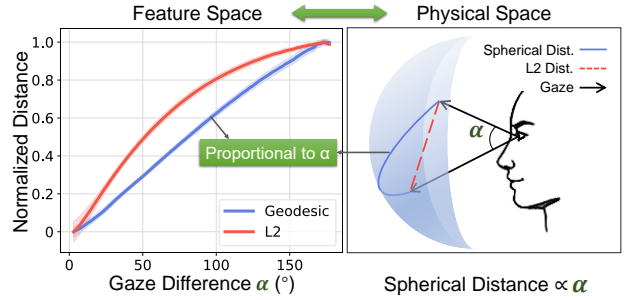


Figure 2. Left: the L2 and geodesic distance with respect to the angular difference between samples in ETH-XGaze dataset. Right: the physics of gaze. The geodesic distance between features and the distance along the spherical surface are proportional to the gaze differences.

rotation by measuring the geodesic distance between eye images [22]. More recently, a number of gaze estimation datasets have been collected [10, 17, 41, 13, 39]. These datasets provide hundreds of thousands of user images with gaze labels, which makes deep learning based gaze estimation possible. Representative studies include gaze estimation using convolutional neural networks (CNNs) [40] with eye images [40, 9] or face images [41, 7, 5, 17, 1]. Some previous studies also represent gaze features as low dimensional manifolds for personalization [24] and unsupervised learning [38]. But these methods still construct manifolds by data-driven learning approach with supervision like gaze redirection. Our method connects gaze feature to 3D space by the physical rules in an unsupervised manner.

2.2. Cross-domain Gaze Estimation

One of the major problem of the deep-learning based approaches is that the performance degrade severely when testing on a different domain. To improve the cross-domain performance, a number of unsupervised domain adaptation methods have been proposed. Liu *et al.* propose to adapt the model to target domain with the guidance of outliers by collaborative learning [21]. Wang *et al.* utilize contrastive learning to pull features with close gaze labels together [35]. Bao *et al.* propose to improve the cross-dataset accuracy by the rotation consistency of gaze [2]. Nevertheless, the above methods require target domain images to train domain specific models, which is infeasible in real world settings, as target domain data is often inaccessible. Recently, Cheng *et al.* propose to improve the generalization ability of gaze estimation model by purifying gaze feature in source domain [6]. Without target domain images, the cross-domain gaze estimation problem is more challenging and remains much space to be explored.

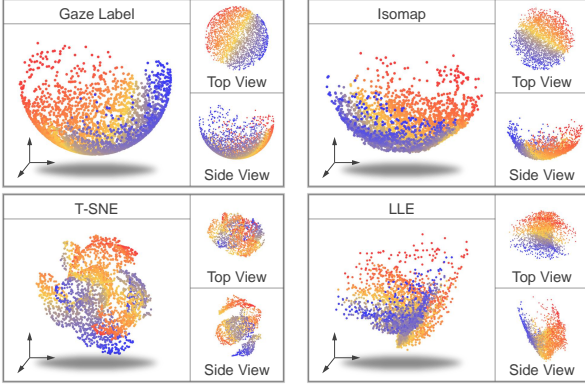


Figure 3. Distribution of gaze feature after dimension reduced to 3D space in ETH-XGaze dataset. Three different unsupervised manifold learning methods (Isomap, T-SNE and LLE) are used. Only the results of Isomap show identical patterns as the gaze ground truth.

3. From Physical Rule to Regression Feature

In this section, we introduce a concept of Physics-Consistent Feature (PCF). Our motivation stems from a straightforward idea, *i.e.*, for a *regression task*, the features extracted by the network may exist in a way that they share the similar numerical patterns with the corresponding physical variables to be regressed. Once these features are discovered, they can be constrained by the same physical rules that lie in original variables. As the physical rules always hold true, this reduces the dependence on ground truth data in conventional methods, and thus helps enhance the interpretability of the algorithm, address the insufficiency of training data, overcome the overfitting problem of the algorithm, and improve the generalization ability.

Motivated by this idea, this section explores the kind of features that should be in line with the laws of eye physiology for the gaze estimation problem. The gaze direction is commonly expressed as a 2D unit vector, so its angular rotation can be modeled as a displacement on a 2D unit sphere embedded in 3D Euclidean space. Thus, although the input to gaze estimation network is image data with million dimensions, its physics-consistent features mainly characterize 2D spherical motion. Consequently, we make the following *Hypothesis*:

Hypothesis 1 *The gaze features extracted from the images can be effectively mapped to the 2D unit spherical surface, and subject to the following physical consistency: the angle between the features (spherical distance) is proportional to the angle between the real-world gaze directions.*

The gaze feature above is the feature extracted by the last convolutional layer of a ResNet-18 network trained on

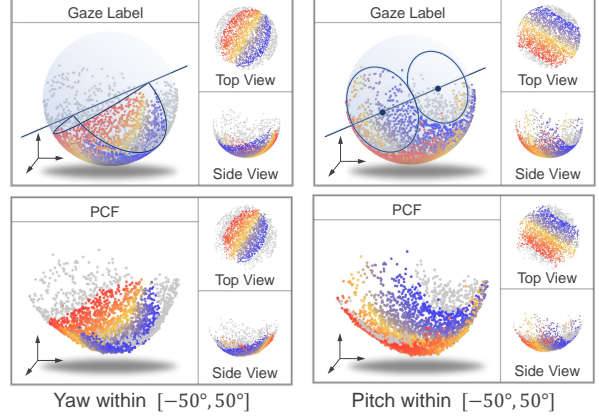


Figure 4. Gaze features after dimension reduction (*i.e.*, PCF) share the same spherical distribution as gaze label. To better demonstrate the similarity, data points within certain gaze range are colored according to the gaze angles. In the visualization of PCF, the gaze pitch and yaw distribute along the longitudinal and latitudinal direction, just like the gaze labels.

gaze estimation dataset, *i.e.* ETH-XGaze. Further details will be introduced in Sec. 4. In the following, we verify this hypothesis and give the computation of such physics-consistent 2D feature.

3.1. Verification of the Hypothesis

We conducted two prove-of-concept experiments to verify the above hypothesis.

First, if the hypothesis holds, the Euclidean distance between features is proportional to the gaze angular difference only when gazes are close enough, *i.e.*,

$$\|\mathbf{f}_i, \mathbf{f}_j\|_2 \propto \text{Ang}(\mathbf{y}_i^s, \mathbf{y}_j^s), \quad (1)$$

where $\text{Ang}(\mathbf{y}_i^s, \mathbf{y}_j^s)$ is the angular difference between gaze ground truth \mathbf{y}_i^s and \mathbf{y}_j^s . For samples with large gaze differences, spherical distances between features should be measured by Geodesic distance:

$$d_G(\mathbf{f}_i, \mathbf{f}_j) \propto \text{Ang}(\mathbf{y}_i^s, \mathbf{y}_j^s), \quad (2)$$

where $d_G(\mathbf{f}_i, \mathbf{f}_j)$ is the geodesic distance between features. A geodesic distance measures the shortest path between two features, and is computed by adding up small Euclidean distances (Eq. (1)) of neighboring features along that path [31]. Relationship in Eq. (2) holds true globally in our hypothesis. As shown in the left part of Fig. 2, the geodesic distance in feature space is linear to gaze differences globally in ETH-XGaze dataset. This numerical relationship of feature space is consistent with physical space, where the spherical distances is linear to gaze differences. The results verify our

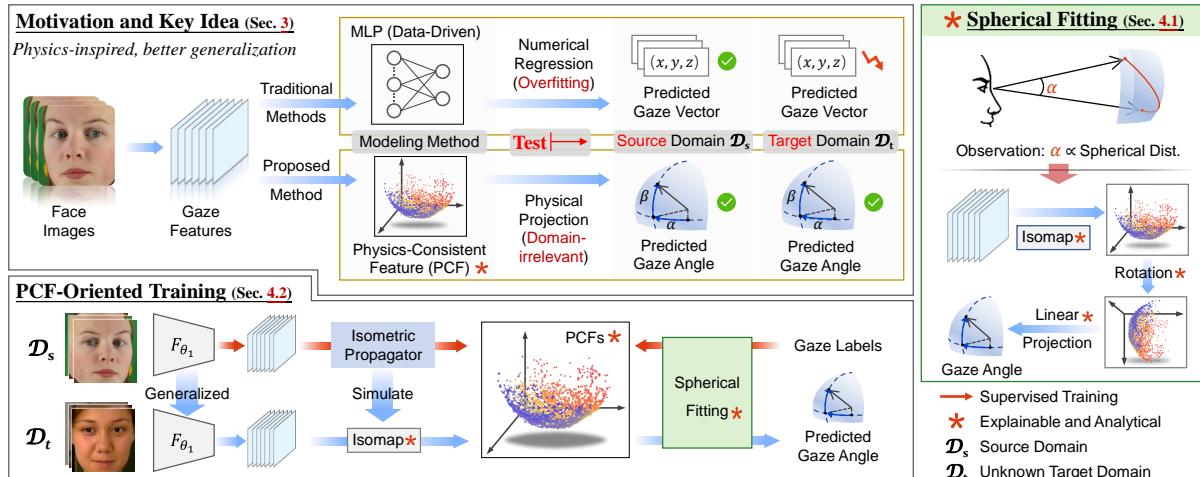


Figure 5. Overview of the proposed PCFGaze framework. The key idea of the PCFGaze framework is to improve the generalization ability by optimizing gaze model through physics of gaze, which is domain irrelevant. Based on the observation that the spherical distance is proportional to the gaze differences, we construct the Physics-Consistent Feature (PCF) that connects gaze feature to the physics of gaze and estimates gaze by Spherical Fitting analytically. With the help of PCF and Spherical Fitting, the PCFGaze framework optimize gaze feature with the physics of gaze by the proposed PCF-Oriented Training for better generalization ability.

hypothesis that gaze feature constitutes a manifold in feature space, and is connected to gaze by geodesic distance.

Second, we map gaze features to 3D space by three different manifold learning methods. Specifically, we use the Isometric map (Isomap) [32], the Local Linear Embedding (LLE) [25] and the T-distributed Stochastic Neighbor Embedding (t-SNE) [33]. The results are shown in Fig. 3. Data points are colored according to the gaze rotation angles. For a more intuitive comparison, we also visualize the distribution of gaze ground truth in the first column. The results of Isomap distribute on a spherical surface, similar to the gaze ground truth. The results are consistent with our hypothesis as the Isomap maps features to low dimensional space according to the geodesic distance between them. To further investigate the distribution pattern, we only color data points within certain gaze range in Fig. 4. It is clear that gaze pitch and yaw distribute along the longitudinal and latitudinal direction of the sphere, which is consistent with the physical definition of gaze. We name the 3D data points of Isomap as Physics-Consistent Feature (PCF). PCF links gaze features to the physical definition of gaze by an intrinsic property of the gaze feature manifold, *i.e.*, the geodesic distance. This insight of gaze features may facilitate the training of gaze estimation models, which will be discussed in next section.

3.2. Benefit of PCF

In this section, we discuss the application of PCF and explain how it differs from common deep learning based gaze estimation approaches. In deep learning based approaches,

gaze features are mapped to gaze directions using an Multi-layer Perceptron (MLP). The MLP is trained based on enormous amount of data with ground truth. Thus, it suffers from the overfitting problem. On the contrary, the proposed PCF connects features to gaze vectors by the intrinsic property of gaze feature manifold in an unsupervised manner. For a given sample, PCF reveals where the ideal gaze feature should be in the feature space, so that it serves as a constraint to optimize gaze features in a more direct and fundamental way.

4. The PCFGaze Framework

The overview of the PCFGaze framework is shown in Fig. 5. Based on the analysis in Sec. 3, we propose Spherical Fitting, which estimates gaze from PCF analytically by physical projection. With the help of PCF, we propose the PCF-Oriented Training, which optimize the gaze feature space with the physic of gaze. As the physical rules are universal, the PCF-Oriented Training improves the generalization ability of gaze estimation model without extra training data.

4.1. Spherical Fitting

As shown in Fig. 4, PCF of the pretrained model shares the same gaze distribution pattern as the ground truth. Thus, we propose Spherical Fitting (SF) algorithm that estimates gaze angles according to the position of PCF analytically. Specifically, we project PCF to a sphere and fit the Euler angles of the projected PCF to gaze angles by linear functions.

Given the source domain $\mathcal{D}_s = \{\mathbf{x}_i^s, \mathbf{y}_i^s\}_{i=1}^{N_s}$ where \mathbf{x}_i^s is the face image and $\mathbf{y}_i^s = (x_i, y_i, z_i)$ is the ground truth gaze direction vector, we pretrain the gaze estimation model by \mathcal{L}_1 loss function:

$$\arg \min_{\theta_1, \theta_2} (\mathcal{L}_1(\mathbf{y}_i^s - L_{\theta_2}(F_{\theta_1}(\mathbf{x}_i^s)))|_{i=1}^{N_s}), \quad (3)$$

where $F_{\theta_1}(\cdot)$ is the feature extractor CNN and $L_{\theta_2}(\cdot)$ is the regression MLP. After the pretrain is completed, PCF \mathbf{f}_{pc} is constructed by performing Isomap on gaze features:

$$\{\mathbf{f}_{pc,i}\}_{i=1}^{N_s} = \text{Isomap}(\{\mathbf{f}_i\}_{i=1}^{N_s}), \quad (4)$$

$$\mathbf{f}_i = F_{\theta_1}(\mathbf{x}_i^s).$$

The Spherical Fitting algorithm estimates gaze from the PCF: $\mathbf{g}_i^s = \text{SF}_{\theta_s}(\mathbf{f}_{pc,i})$. To do so, we project \mathbf{f}_{pc} to a sphere with center \mathbf{O}_c and rotate it so that the orientation of the sphere could be aligned with gaze:

$$(\mathbf{f}'_{pc,i})^T = \mathbf{R}(\mathbf{f}_{pc,i} - \mathbf{O}_c)^T = (x'_i, y'_i, z'_i)^T, \quad (5)$$

where \mathbf{R} is the rotation matrix. The gaze estimation $\mathbf{g}_i^s = (\alpha_i, \beta_i)$ is the linear projections of the Euler angles of \mathbf{f}'_{pc} :

$$\alpha_i = k_1 \arctan\left(\frac{-x'_i}{-z'_i}\right) + b_1, \quad (6)$$

$$\beta_i = k_2 \arcsin(-y'_i) + b_2.$$

Following the insight that geodesic distance between features is proportional to the gaze differences between samples, we estimate gaze directions from the gaze feature analytically by the proposed Spherical Fitting algorithm. The Spherical Fitting algorithm consists of 10 parameters $\theta_s = (\mathbf{O}_c, \mathbf{R}, k_1, k_2, b_1, b_2)$. These parameters are determined by optimizing the angular error between gaze estimation and ground truth \mathbf{y}^s :

$$\arg \min_{\theta_s} (\text{Ang}(\mathbf{g}_i^s, \mathbf{y}_i^s)|_{i=1}^{N_s}). \quad (7)$$

In practice, we randomly choose a subset of 2000 samples from the source domain for parameter optimization considering the time demand of Isomap. During inference, features of the new samples are concatenated to the geodesic distance map built in the training phase, which could be done in real time. Spherical Fitting algorithm generalizes well to target domains because the physics of gaze hold true globally.

4.2. PCF-Oriented Training

Our ultimate goal is to train the feature extractor F_{θ_1} under the guidance of the Spherical Fitting algorithm. Unfortunately, Isomap is hard to integrate to the back propagation process because it is both time and space consuming. The time complexity of Isomap is $N^2 \log N$ and the space

demand is N^2 , where N is the number of samples. The time and memory space required by the Isomap to process hundreds of thousands of gaze features is enormous. Thus, we propose the PCF-Oriented Training (IT) method to solve this problem.

In PCF-Oriented Training phase, we train a Isometric Propagator to replace the Isomap algorithm. First, we perform Isomap on a subset of source domain with N' samples:

$$\{\mathbf{f}_{pc,i}\}_{i=1}^{N'} = \text{Isomap}(\{\mathbf{f}_i\}_{i=1}^{N'}). \quad (8)$$

N' is set to 2000 as it is enough to cover the common gaze range. Then, we train a simple three layer MLP as the Isometric Propagator $\text{IP}_{\theta_3}(\cdot)$ to replace the Isomap algorithm. $\text{IP}_{\theta_3}(\cdot)$ is supervised by \mathcal{L}_1 loss function:

$$\arg \min_{\theta_3} (\mathcal{L}_1(\mathbf{f}_{pc,i}, \text{IP}_{\theta_3}(\mathbf{f}_i))|_{i=1}^{N'}). \quad (9)$$

The idea is to simulate the Isomap algorithm by training the Isometric Propagator. During PCF-Oriented Training, PCF is derived by the Isometric Propagator instead of Isomap algorithm: $\mathbf{f}_{pc,i} = \text{IP}_{\theta_3}(\mathbf{f}_i)$. After the training of Isometric Propagator, we freeze the parameters of it and optimize the model by constraining PCF. As the Spherical Fitting algorithm is analytical, we inversely calculate the ground truth PCF $\hat{\mathbf{f}}_{pc,i}$ from the gaze ground truth:

$$\hat{\mathbf{f}}_{pc,i} = \text{SF}_{\theta_s}^{-1}(\mathbf{y}_i). \quad (10)$$

Finally, we retrain the feature extractor by constraining the PCF with \mathcal{L}_1 loss function:

$$\arg \min_{\theta_1} (\mathcal{L}_1(\hat{\mathbf{f}}_{pc,i}, \text{IP}_{\theta_3}(F_{\theta_1}(\mathbf{x}_i)))|_{i=1}^{N_s}). \quad (11)$$

In this way, we directly optimize gaze features according to their relation to physical definition of gaze. As the optimization objective of the gaze features is to match the distribution modeled by PCF and Spherical Fitting, user gaze is estimated by Isomap and SF_{θ_s} at inference time:

$$\mathbf{g}_i = \text{SF}_{\theta_s}(\text{Isomap}(F_{\theta_1}(\mathbf{x}_i))). \quad (12)$$

4.3. Implementation Details

We employ PyTorch for implementation. ResNet 18 is used as the baseline following previous studies [6, 35, 2]. For the training of the pretrain model, IP and PCF-Oriented Training, we use the Adam optimizer with a learning rate of 10^{-4} . The model is pretrained for 10 epochs. The PCF-Oriented Training is also 10 epochs, while the IP is trained for 100 epochs. For Isomap, we use the implementation of Scikit-learn. The number of neighbor in geodesic distance is set to 300 by default.

Table 1. Cross-domain gaze estimation error in degrees. The proposed PCFGaze method achieves improvements as large as 29.23% without any extra training data. Percentage with underline indicates the largest improvement over corresponding baseline. Bold number indicates the lowest estimation error. * means that the number of neighbors in geodesic distance is customized for each source domain (100, 800 and 300 for \mathcal{D}_E , \mathcal{D}_G and \mathcal{D}_M respectively). In row 5, the number is set to 300 for all source domain as default.

Method	$\mathcal{D}_E \rightarrow \mathcal{D}_M$	$\mathcal{D}_E \rightarrow \mathcal{D}_D$	$\mathcal{D}_G \rightarrow \mathcal{D}_M$	$\mathcal{D}_G \rightarrow \mathcal{D}_D$	$\mathcal{D}_M \rightarrow \mathcal{D}_E$	$\mathcal{D}_M \rightarrow \mathcal{D}_G$	$\mathcal{D}_M \rightarrow \mathcal{D}_D$
1 Baseline [6]	8.13	7.74	9.89	11.42	-	-	-
2 PureGaze [6]	7.08 \blacktriangledown 12.92%	7.48 \blacktriangledown 3.36%	9.28 \blacktriangledown 6.17%	9.32 \blacktriangledown 18.39%	-	-	-
3 Baseline	8.64	7.83	8.68	12.35	14.03	15.48	16.15
4 Baseline+SF	7.92	8.22	8.33	11.40	14.14	14.83	11.80
5 PCFGaze	7.40 \blacktriangledown 14.35%	7.30 \blacktriangledown 6.77%	8.36 \blacktriangledown 3.69%	10.18 \blacktriangledown 17.57%	13.69 \blacktriangledown 2.42%	13.76 \blacktriangledown 11.11%	12.40 \blacktriangledown 23.22%
6 Baseline+SF*	7.98	8.45	7.79	10.97	14.14	14.83	11.80
7 PCFGaze*	7.00 \blacktriangledown <u>18.98%</u>	7.02 \blacktriangledown <u>10.34%</u>	7.71 \blacktriangledown <u>11.18%</u>	8.74 \blacktriangledown <u>29.23%</u>	13.69 \blacktriangledown <u>2.42%</u>	13.76 \blacktriangledown <u>11.11%</u>	12.40 \blacktriangledown <u>23.22%</u>

Table 2. Cross domain gaze estimation error in degrees. † indicates that the method employs ResNet-50 as backbone. The proposed PCFGaze improves accuracy of different baseline model and outperforms other SOTA methods.

Method	$\mathcal{D}_E \rightarrow \mathcal{D}_M$	$\mathcal{D}_E \rightarrow \mathcal{D}_D$	$\mathcal{D}_G \rightarrow \mathcal{D}_M$	$\mathcal{D}_G \rightarrow \mathcal{D}_D$
Full-Face[41]	12.35	30.15	11.13	14.42
ADL[13]	7.23	8.02	11.36	11.86
CA-Net[7]	-	-	27.13	31.41
LatentGaze[19]	7.98	9.81	-	-
PureGaze[6]	7.08	7.48	9.28	9.32
Baseline	8.64	7.83	8.68	12.35
PCFGaze	7.40	7.30	8.36	10.18
Baseline†	7.3	8.43	8.22	11.79
PCFGaze†	6.15	7.66	7.61	11.42

5. Experiments

5.1. Data Preparation

We conduct experiments on four commonly used gaze estimation datasets: ETH-XGaze (\mathcal{D}_E) [39], Gaze360 (\mathcal{D}_G) [13], MPIIFaceGaze (\mathcal{D}_M) [41] and EyeDiap (\mathcal{D}_D) [10]. We pre-process the data following the techniques in [21, 8].

ETH-XGaze: 756k images captured by high resolution cameras in laboratory environment with large gaze range.

Gaze360: 101k images captured by a 360° camera on streets with large gaze range.

MPIIFaceGaze: 45k images captured by web camera during daily usage of laptop computers. The gaze range of \mathcal{D}_M is less than half the range of \mathcal{D}_E and \mathcal{D}_G . Thus, in $\mathcal{D}_M \rightarrow \mathcal{D}_E$ and $\mathcal{D}_M \rightarrow \mathcal{D}_G$ settings, we only use samples within the gaze range of \mathcal{D}_M for testing.

EyeDiap: 16k images captured under laboratory environment with screen and floating targets. As the number of images is significantly less than other datasets, we only use \mathcal{D}_D as target domain.

In addition, the cross-domain error between \mathcal{D}_E and \mathcal{D}_G is extremely large (around 20°). Thus, we exclude the $\mathcal{D}_E \rightarrow \mathcal{D}_G$ and $\mathcal{D}_G \rightarrow \mathcal{D}_E$ settings in our experiments, which is also excluded in previous studies [34, 21, 2, 6].

5.2. Performance of PCFGaze Framework

5.2.1 Domain Generalization Accuracy

To test the generalization ability of the PCFGaze framework, we conduct experiments in 6 different cross domain settings. The results are shown in Tab. 1. To make a fair comparison with [6], we provide the error of baseline reported in the original paper and the percentage of improvements. The PCFGaze framework in the default setting achieves stable improvements in all 7 settings, proves the effectiveness of the PCFGaze framework. Compared to the baseline model, the proposed framework achieves 23.22% improvement in $\mathcal{D}_M \rightarrow \mathcal{D}_D$ setting. Row 4 of Tab. 1 shows that without PCF-Oriented Training, the proposed Spherical Fitting still improves the cross domain performance in most settings (5 out of 7). These results prove our point in Sec. 3.2 that by estimating gaze analytically through the physics of gaze, Spherical Fitting is less affected by overfitting than the regression MLP. The performance of PCFGaze is further improved by tuning the number of neighbors in geodesic distance for each source domain. The numbers of neighbors are set to 100, 800 and 300 for \mathcal{D}_E , \mathcal{D}_G and \mathcal{D}_M respectively. As shown in the row 7 of Tab. 1, the improvements PCFGaze* brought are over 50% more than PureGaze.

In Tab. 2, we compare the PCFGaze with SOTA gaze estimation methods [41, 13, 7] and gaze generalization methods [6, 19]. For [41, 13, 7, 6], we report the cross-domain accuracy from [6]. We report the accuracy of [19] from the original paper. The results indicate that the proposed PCFGaze outperforms SOTA gaze estimation and gaze generalization methods. Results in the bottom rows also show that PCFGaze achieves stable improvement across differ-

Table 3. The mean and standard deviation of the estimation error for last 5 epochs. The proposed PCFGaze are not only more accurate but also more stable than the baseline. The Spherical Fitting is also more stable than the regression MLP by estimating gaze analytically based on physics of gaze.

Method	$\mathcal{D}_E \rightarrow \mathcal{D}_M$	$\mathcal{D}_E \rightarrow \mathcal{D}_D$	$\mathcal{D}_G \rightarrow \mathcal{D}_M$	$\mathcal{D}_G \rightarrow \mathcal{D}_D$
Baseline	8.66±0.52	7.76±0.83	8.59±0.65	10.87±1.40
Baseline+SF	7.88±0.21	7.72±0.30	8.57±0.39	10.94±0.80
PCFGaze	7.44±0.16	7.3±0.12	8.33±0.29	9.35±0.82

Table 4. Additional experiments: fine-tuning models with 100 target domain images for domain specific generalization

Method	$\mathcal{D}_E \rightarrow \mathcal{D}_M$	$\mathcal{D}_E \rightarrow \mathcal{D}_D$	$\mathcal{D}_G \rightarrow \mathcal{D}_M$	$\mathcal{D}_G \rightarrow \mathcal{D}_D$
Baseline	8.64	7.83	8.68	12.35
Fine-tune	5.11	5.92	5.59	6.30
PCFGaze-Ft	4.74	5.88	5.41	6.39

ent backbone models (ResNet-18 and ResNet-50). Overall, above experiments prove that the PCFGaze effectively improves the cross-domain gaze estimation accuracy.

5.2.2 Stability of the PCFGaze

In practical settings, target domains are often unknown, makes the stability of the model critical. Stable performance across different epochs means less risk of randomly stopping at an epoch with large estimation error. To verify the stability of the PCFGaze, we calculate the mean and standard deviation (std.) of the gaze estimation error for different methods in Tab. 3. We choose the last 5 epochs to make sure the model is converged. Results show that the std. of PCFGaze is less than half of the baseline in most settings (3 out of 4). Besides, although the accuracy of Spherical Fitting is similar to the regression MLP (baseline) without PCF-Oriented Training, it still appear to be much more stable because Spherical Fitting estimates gaze analytically from physical rules instead of data-driven methods. Note we strictly follow the cross-domain condition and report the accuracy of the last epoch in Tab. 1 and Tab. 2.

5.2.3 Additional Experiment: Domain Adaptation with Target Domain Data

Results in Sec. 5.2.1 show that the PCFGaze framework improves the generalization ability significantly without target domain data. To further prove the advantage of PCFGaze framework, we conduct additional domain adaptation experiments with 100 target domain images. We fine-tune the baseline model with a learning rate of $5 * 10^{-5}$ for 50 epochs in target domain. For PCFGaze, we train the model following the PCF-Oriented Training for 30 epochs

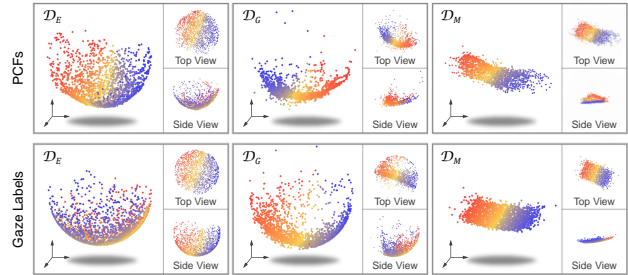


Figure 6. Visualization of the PCF and gaze label from \mathcal{D}_E , \mathcal{D}_G and \mathcal{D}_M . PCF from three datasets all share the same distribution pattern with gaze ground truth despite significant differences (image quality, head poses, gaze range, etc.) between datasets. It proves the generalization ability of PCFGaze.

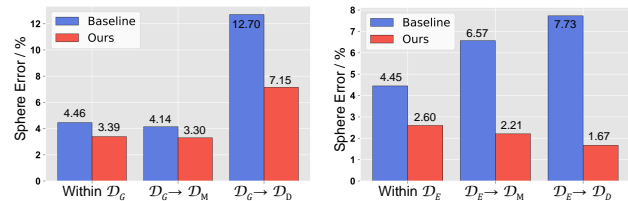


Figure 7. The Sphere Error of the SF before (Baseline) and after PCF-Oriented Training (Ours). Smaller sphere error indicates that the PCFs are more consistent with the physics of gaze after PCF-Oriented Training.

and calculate parameters of Spherical Fitting with the 100 target domain images, which is named PCFGaze-Ft. The results are shown in Tab. 4. The PCFGaze-Ft outperforms fine-tune method in most settings. The results validate the advantage of PCFGaze over fine-tune method in supervised domain adaptation with small amount of samples (100), although PCFGaze is not designed for such purpose.

5.3. Verification of the PCFGaze

In Sec. 5.2, we show the effectiveness of the PCFGaze by cross domain gaze estimation accuracy. In this section, we verify the idea behind PCFGaze. The PCFGaze works only if the following propositions hold true: 1) PCF shares the same gaze distribution pattern as the gaze label; 2) PCF-Oriented Training constrains the model to extract more physics-consistent features. We verify these two key propositions statistically and intuitively in this section.

Proposition (1). Fig. 4 proves that PCFs in \mathcal{D}_E share the same gaze distribution pattern as the gaze label, we further analyze PCFs in other within and cross dataset settings. We visualize PCFs of the baseline model in \mathcal{D}_E , \mathcal{D}_G and \mathcal{D}_M under within dataset settings in Fig. 6. It is clear that the shape and range of PCFs is consistent with gaze labels.

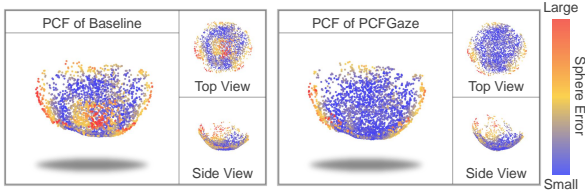


Figure 8. Visualization of the Sphere Error before and after PCF-Oriented Training in \mathcal{D}_E . The Sphere Error of PCFGaze is obviously smaller, proves that gaze feature extracted by PCFGaze is more consistent with gaze ground truth.

The gaze (visualized in different color) changes smoothly along the spherical surface of PCFs, proves that the PCF is well-connected to gaze. Fig. 6 proves that the Hypothesis 1 holds true when the image quality and gaze range of the training dataset change dramatically. For PCFs under cross dataset settings, results in row 4 and 6 of Tab. 1 already show that PCF is well mapped to gaze by Spherical Fitting, *i.e.*, rotation and linear fitting in all cross domain settings. Thus, proposition (1) holds true in both within and cross dataset settings.

Proposition (2). We verify proposition (2) by analyzing whether the extracted features after PCF-Oriented Training are more consistent with the physics of gaze. As high dimensional features are hard to visualize and understand, we analyze PCFs for replacement. To see how consistent PCFs are with the physics of gaze, we measure how spherical PCFs are by calculating the Sphere Error, *i.e.*, the average distance from PCFs to the spherical surface. As shown in Fig. 7, the Sphere Error of the PCFGaze is lower than the baseline in both within and cross domain settings. For more intuitive understanding, we visualize the Sphere Error of PCFs from \mathcal{D}_E before and after PCF-Oriented Training. The Sphere Error is significantly reduced in the center area after PCF-Oriented Training. Besides, the side views also show that the surface of the PCFs after PCF-Oriented Training is more spherical. Thus, we verify that proposition (2) holds true from both objective and subjective perspectives.

5.4. Additional Application of PCFGaze: Data Analysis

As the PCFGaze reveals how gaze feature is connected to the physics of gaze in an analytical way, ideas behind PCFGaze could also serve as criteria during data analysis. In Fig. 9, we visualize the \mathcal{L}_2 and geodesic distances with respect to the gaze difference between samples from \mathcal{D}_E , \mathcal{D}_G and \mathcal{D}_M . The results show the obvious differences between datasets. Eq. (2) holds true across all sample pairs in \mathcal{D}_E . We assume it is because the high resolution and the controlled environment during collecting. For \mathcal{D}_G , the

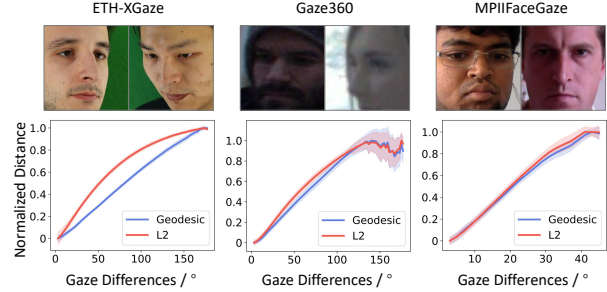


Figure 9. The \mathcal{L}_2 and Geodesic distances between gaze features with respect to the angular difference between samples from \mathcal{D}_E , \mathcal{D}_G and \mathcal{D}_M .

pattern become random and the std increases dramatically when the gaze differences exceed 120° . We assume the possible reason is that the quality of samples in the edge of the gaze range decreases, makes the corresponding features more random. For \mathcal{D}_M , the pattern is less obvious. One possible reason is that the narrow gaze range of \mathcal{D}_M could be seen as a small neighbor area compared to other two dataset. Overall, Fig. 9 shows that the feature space of \mathcal{D}_E is more consistent with the gaze physics. Correspondingly, the \mathcal{D}_E baseline performs the best in cross-domain evaluation.

6. Limitations and Future Work

The PCFGaze successfully alleviates one of the major challenges in cross-domain settings, *i.e.*, the absence of target domain data. Another challenge is that the gaze range of domains are different. The improvement of PCFGaze is less obvious if the gaze range of the target domain is significantly larger than the source domain. Existing methods still can not handle such problem well. Although theoretically the Spherical Fitting is capable of estimating unseen gaze range, the feature extractor can not handle samples with unseen gaze range correctly. In the future, we may dive deeper to the gaze feature space and try to tackle this problem.

7. Conclusion

In this paper, we propose the PCFGaze framework to increase the generalization ability of gaze estimation models without target domain data. We connect gaze features to the physics of gaze analytically through PCF, and constrains the gaze estimation model by the physics of gaze. As the physics of gaze is fundamental and explainable, the constrain of PCFGaze is less affected by the overfitting problem. Experimental results show that the PCFGaze framework improves accuracy in 8 different cross-domain settings. The idea of PCF may inspire method design for other physical related regression tasks such as pose estimation.

References

- [1] Yiwei Bao, Yihua Cheng, Yunfei Liu, and Feng Lu. Adaptive feature fusion network for gaze tracking in mobile tablets. In *2020 25th International Conference on Pattern Recognition (ICPR)*, pages 9936–9943. IEEE, 2021. [2](#)
- [2] Yiwei Bao, Yunfei Liu, Haofei Wang, and Feng Lu. Generalizing gaze estimation with rotation consistency. In *Proceedings of the IEEE/CVF Conference on Computer Vision and Pattern Recognition*, pages 4207–4216, 2022. [2](#), [5](#), [6](#)
- [3] Alisa Burova, John Mäkelä, Jaakko Hakulinen, Tuuli Keskinen, Hanna Heinonen, Sanni Siltanen, and Markku Turunen. Utilizing vr and gaze tracking to develop ar solutions for industrial maintenance. In *Proceedings of the 2020 CHI Conference on Human Factors in Computing Systems*, pages 1–13, 2020. [1](#)
- [4] Nora Castner, Thomas C Kuebler, Katharina Scheiter, Juliane Richter, Thérèse Eder, Fabian Hüttig, Constanze Keutel, and Enkelejda Kasneci. Deep semantic gaze embedding and scanpath comparison for expertise classification during opt viewing. In *ACM Symposium on Eye Tracking Research and Applications*, pages 1–10, 2020. [1](#)
- [5] Zhaokang Chen and Bertram E Shi. Appearance-based gaze estimation using dilated-convolutions. In *Asian Conference on Computer Vision*, pages 309–324. Springer, 2018. [2](#)
- [6] Yihua Cheng, Yiwei Bao, and Feng Lu. Puregaze: Purifying gaze feature for generalizable gaze estimation. In *Proceedings of the AAAI Conference on Artificial Intelligence*, volume 36, pages 436–443, 2022. [1](#), [2](#), [5](#), [6](#)
- [7] Yihua Cheng, Shiyao Huang, Fei Wang, Chen Qian, and Feng Lu. A coarse-to-fine adaptive network for appearance-based gaze estimation. In *Proceedings of the AAAI Conference on Artificial Intelligence*, volume 34, pages 10623–10630, 2020. [2](#), [6](#)
- [8] Yihua Cheng, Haofei Wang, Yiwei Bao, and Feng Lu. Appearance-based gaze estimation with deep learning: A review and benchmark. *arXiv preprint arXiv:2104.12668*, 2021. [6](#)
- [9] Yihua Cheng, Xucong Zhang, Feng Lu, and Yoichi Sato. Gaze estimation by exploring two-eye asymmetry. *IEEE Transactions on Image Processing*, 29:5259–5272, 2020. [2](#)
- [10] Kenneth Alberto Funes Mora, Florent Monay, and Jean-Marc Odobez. Eyediap: A database for the development and evaluation of gaze estimation algorithms from rgb and rgb-d cameras. In *Proceedings of the Symposium on Eye Tracking Research and Applications*, pages 255–258, 2014. [2](#), [6](#)
- [11] Elias Daniel Guestrin and Moshe Eizenman. General theory of remote gaze estimation using the pupil center and corneal reflections. *IEEE Transactions on biomedical engineering*, 53(6):1124–1133, 2006. [2](#)
- [12] Dan Witzner Hansen and Qiang Ji. In the eye of the beholder: A survey of models for eyes and gaze. *IEEE transactions on pattern analysis and machine intelligence*, 32(3):478–500, 2009. [2](#)
- [13] Petr Kellnhofer, Adria Recasens, Simon Stent, Wojciech Matusik, and Antonio Torralba. Gaze360: Physically unconstrained gaze estimation in the wild. In *Proceedings of the IEEE/CVF International Conference on Computer Vision*, pages 6912–6921, 2019. [1](#), [2](#), [6](#)
- [14] Jess Kerr-Gaffney, Amy Harrison, and Kate Tchanturia. Eye-tracking research in eating disorders: A systematic review. *International Journal of Eating Disorders*, 52(1):3–27, 2019. [1](#)
- [15] Andrew J King, Gregory F Cooper, Gilles Clermont, Harry Hochheiser, Milos Hauskrecht, Dean F Sittig, and Shyam Visweswaran. Leveraging eye tracking to prioritize relevant medical record data: comparative machine learning study. *Journal of medical Internet research*, 22(4):e15876, 2020. [1](#)
- [16] Robert Konrad, Anastasios Angelopoulos, and Gordon Wetstein. Gaze-contingent ocular parallax rendering for virtual reality. *ACM Transactions on Graphics (TOG)*, 39(2):1–12, 2020. [1](#)
- [17] Kyle Krafka, Aditya Khosla, Petr Kellnhofer, Harini Kannan, Suchendra Bhandarkar, Wojciech Matusik, and Antonio Torralba. Eye tracking for everyone. In *Proceedings of the IEEE conference on computer vision and pattern recognition*, pages 2176–2184, 2016. [2](#)
- [18] Mikko Kytö, Barrett Ens, Thammathip Piumsomboon, Gun A Lee, and Mark Billinghurst. Pinpointing: Precise head-and eye-based target selection for augmented reality. In *Proceedings of the 2018 CHI Conference on Human Factors in Computing Systems*, pages 1–14, 2018. [1](#)
- [19] Isack Lee, Jun-Seok Yun, Hee Hyeon Kim, Youngju Na, and Seok Bong Yoo. Latentgaze: Cross-domain gaze estimation through gaze-aware analytic latent code manipulation. In *Proceedings of the Asian Conference on Computer Vision*, pages 3379–3395, 2022. [6](#)
- [20] Jiahui Liu, Jiannan Chi, and Shuo Fan. A method for accurate 3d gaze estimation with a single camera and two collinear light sources. *IEEE Transactions on Instrumentation and Measurement*, 2022. [2](#)
- [21] Yunfei Liu, Ruicong Liu, Haofei Wang, and Feng Lu. Generalizing gaze estimation with outlier-guided collaborative adaptation. In *Proceedings of the IEEE/CVF International Conference on Computer Vision*, pages 3835–3844, 2021. [1](#), [2](#), [6](#)
- [22] Feng Lu, Xiaowu Chen, and Yoichi Sato. Appearance-based gaze estimation via uncalibrated gaze pattern recovery. *IEEE Transactions on Image Processing*, 26(4):1543–1553, 2017. [2](#)
- [23] Feng Lu, Yusuke Sugano, Takahiro Okabe, and Yoichi Sato. Adaptive linear regression for appearance-based gaze estimation. *IEEE transactions on pattern analysis and machine intelligence*, 36(10):2033–2046, 2014. [2](#)
- [24] Seonwook Park, Shalini De Mello, Pavlo Molchanov, Umar Iqbal, Otmar Hilliges, and Jan Kautz. Few-shot adaptive gaze estimation. In *Proceedings of the IEEE/CVF international conference on computer vision*, pages 9368–9377, 2019. [2](#)
- [25] Sam T Roweis and Lawrence K Saul. Nonlinear dimensionality reduction by locally linear embedding. *science*, 290(5500):2323–2326, 2000. [4](#)
- [26] Timo Schneider, Boris Schauerte, and Rainer Stiefelhagen. Manifold alignment for person independent appearance-

- based gaze estimation. In *2014 22nd international conference on pattern recognition*, pages 1167–1172. IEEE, 2014. [2](#)
- [27] Vincent Sitzmann, Ana Serrano, Amy Pavel, Maneesh Agrawala, Diego Gutierrez, Belen Masia, and Gordon Wetstein. Saliency in vr: How do people explore virtual environments? *IEEE transactions on visualization and computer graphics*, 24(4):1633–1642, 2018. [1](#)
- [28] Sophie Stellmach, Sebastian Stober, Andreas Nürnberger, and Raimund Dachsel. Designing gaze-supported multimodal interactions for the exploration of large image collections. In *Proceedings of the 1st Conference on Novel Gaze-Controlled Applications*, NGCA '11, New York, NY, USA, 2011. Association for Computing Machinery. [1](#)
- [29] Li Sun, Zicheng Liu, and Ming-Ting Sun. Real time gaze estimation with a consumer depth camera. *Information Sciences*, 320:346–360, 2015. [2](#)
- [30] Kentaro Takemura and Kenta Yamagishi. A hybrid eye-tracking method using a multispectral camera. In *2017 IEEE International Conference on Systems, Man, and Cybernetics (SMC)*, pages 1529–1534. IEEE, 2017. [2](#)
- [31] Joshua B Tenenbaum, Vin de Silva, and John C Langford. A global geometric framework for nonlinear dimensionality reduction. *science*, 290(5500):2319–2323, 2000. [3](#)
- [32] Joshua B Tenenbaum, Vin de Silva, and John C Langford. A global geometric framework for nonlinear dimensionality reduction. *science*, 290(5500):2319–2323, 2000. [4](#)
- [33] Laurens Van der Maaten and Geoffrey Hinton. Visualizing data using t-sne. *Journal of machine learning research*, 9(11), 2008. [4](#)
- [34] Kang Wang, Rui Zhao, Hui Su, and Qiang Ji. Generalizing eye tracking with bayesian adversarial learning. In *Proceedings of the IEEE/CVF Conference on Computer Vision and Pattern Recognition*, pages 11907–11916, 2019. [1](#), [6](#)
- [35] Yaoming Wang, Yangzhou Jiang, Jin Li, Bingbing Ni, Wenrui Dai, Chenglin Li, Hongkai Xiong, and Teng Li. Contrastive regression for domain adaptation on gaze estimation. In *Proceedings of the IEEE/CVF Conference on Computer Vision and Pattern Recognition*, pages 19376–19385, 2022. [1](#), [2](#), [5](#)
- [36] Zhimin Wang, Huangyue Yu, Haofei Wang, Zongji Wang, and Feng Lu. Comparing single-modal and multimodal interaction in an augmented reality system. In *2020 IEEE International Symposium on Mixed and Augmented Reality Adjunct, ISMAR 2020 Adjunct, Recife, Brazil, November 9-13, 2020*, pages 165–166. IEEE, 2020. [1](#)
- [37] Xuehan Xiong, Zicheng Liu, Qin Cai, and Zhengyou Zhang. Eye gaze tracking using an rgbd camera: A comparison with a rgb solution. In *Proceedings of the 2014 ACM International Joint Conference on Pervasive and Ubiquitous Computing: Adjunct Publication*, pages 1113–1121, 2014. [2](#)
- [38] Yu Yu and Jean-Marc Odobez. Unsupervised representation learning for gaze estimation. In *Proceedings of the IEEE/CVF Conference on Computer Vision and Pattern Recognition*, pages 7314–7324, 2020. [2](#)
- [39] Xucong Zhang, Seonwook Park, Thabo Beeler, Derek Bradley, Siyu Tang, and Otmar Hilliges. Eth-xgaze: A large scale dataset for gaze estimation under extreme head pose and gaze variation. In *European Conference on Computer Vision*, pages 365–381. Springer, 2020. [2](#), [6](#)
- [40] Xucong Zhang, Yusuke Sugano, Mario Fritz, and Andreas Bulling. Appearance-based gaze estimation in the wild. In *Proceedings of the IEEE conference on computer vision and pattern recognition*, pages 4511–4520, 2015. [2](#)
- [41] Xucong Zhang, Yusuke Sugano, Mario Fritz, and Andreas Bulling. It’s written all over your face: Full-face appearance-based gaze estimation. In *Proceedings of the IEEE Conference on Computer Vision and Pattern Recognition Workshops*, pages 51–60, 2017. [2](#), [6](#)